UC Santa Barbara
UC Santa Barbara Previously Published Works

Title

Liquid-liquid phase separation of Tau by self and complex coacervation.

Permalink

https://escholarship.org/uc/item/70t1994c

Journal

Protein Science, 30(7)

Authors

Najafi, Saeed

Lin, Yanxian

Longhini, Andrew

et al.

Publication Date

DOI

Peer reviewed

FULL-LENGTH PAPER

Liquid–liquid phase separation of Tau by self and complex coacervation

Saeed Najafi[1,6] | Yanxian Lin[2] | Andrew P. Longhini[4] | Xuemei Zhang[5] | Kris T. Delaney[6] | Kenneth S. Kosik[4,5] | Glenn H. Fredrickson[6,7] | Joan-Emma Shea[1,3] | Songi Han[1,5,7] ᴵᴰ

[1]Department of Chemistry and Biochemistry, University of California Santa Barbara, Santa Barbara, California

[2]Department of Biomolecular Science and Engineering, University of California Santa Barbara, Santa Barbara, California

[3]Department of Physics, University of California at Santa Barbara, Santa Barbara, California

[4]Molecular, Cell and Developmental Biology, University of California Santa Barbara, Santa Barbara, California

[5]Neuroscience Research Institute, University of California Santa Barbara, Santa Barbara, California

[6]Materials Research Laboratory, University of California Santa Barbara, Santa Barbara, California

[7]Department of Chemical Engineering, University of California Santa Barbara, Santa Barbara, California

Correspondence
Songi Han, Department of Chemistry and Biochemistry, University of California Santa Barbara, Santa Barbara, CA 93106. Email: songi@chem.ucsb.edu

Funding information
National Institute of Health, Grant/Award Numbers: GM136411, R01AG05605; National Science Foundation, Grant/ Award Numbers: CNS-1725797, DMR 1720256, DMR-1720256, MCA05S027, MCB-1716956

Abstract

The liquid–liquid phase separation (LLPS) of Tau has been postulated to play a role in modulating the aggregation property of Tau, a process known to be critically associated with the pathology of a broad range of neurodegenerative diseases including Alzheimer's Disease. Tau can undergo LLPS by homotypic interaction through self-coacervation (SC) or by heterotypic association through complex-coacervation (CC) between Tau and binding partners such as RNA. What is unclear is in what way the formation mechanisms for self and complex coacervation of Tau are similar or different, and the addition of a binding partner to Tau alters the properties of LLPS and Tau. A combination of *in vitro* experimental and computational study reveals that the primary driving force for both Tau CC and SC is electrostatic interactions between Tau-RNA or Tau-Tau macromolecules. The liquid condensates formed by the complex coacervation of Tau and RNA have distinctly higher micro-viscosity and greater thermal stability than that formed by the SC of Tau. Our study shows that subtle changes in solution conditions, including molecular crowding and the presence of binding partners, can lead to the formation of different types of Tau condensates with distinct micro-viscosity that can coexist as persistent and immiscible entities in solution. We speculate that the formation, rheological properties and stability of Tau droplets can be readily tuned by cellular factors, and that liquid condensation of Tau can alter the conformational equilibrium of Tau.

KEYWORDS

coacervation, LLPS, neurodegenerative disease, protein aggregation, protein droplets, tauopathy

1 | INTRODUCTION

Tau—an intrinsically disordered protein (IDP)—lacks a well-defined tertiary state that undergoes rapid segmental diffusion and conformational remodeling. The nature of this intrinsic disorder paired with a highly charged amino acid composition offers ample opportunity for Tau molecules to engage in multivalent molecular interactions with itself and many other biomolecular constituents within the cell. Adverse conditions, by mechanisms not

well understood, can lead to the self-assembly and subsequent fibrillization of Tau into a cross β-sheet structure,[1,2] a hallmark of Alzheimer's neurofibrillary tangles.[3,4] Tau has been mainly characterized as a microtubule binding protein, with most of the protein localized to the axons of neurons. However, Tau can also be found off microtubules and can contribute to important cellular responses in the presence of biomolecular signals. For example, Tau interacts with Tyrosine kinase Fyn[5] and the scaffolding protein PSD-95 in dendrites,[6] bundles actin filaments,[7–10] binds to lipid membranes,[11] associates with RNA, in particular tRNA,[3,12] and partitions into stress granules.[13] In a disease state, Tau moves from the axon into the soma and forms inclusion bodies[14] that colocalize non-Tau biomolecules which are hypothesized to be cofactors of pathological fibrilization processes.[2,15–19] Tau is subject to intensive post-translation modifications (PTMs) including hyperphosphorylation, acetylation, ubiquitination, and sumoylation which have been found to be correlated with, or protective of, AD disease progression.[20,21] The non-polar residues of Tau such as leucine, valine and tyrosine, due to the lack of hydrogen bonds with water, can effectively dehydrate the Tau protein (deplete water molecules from its hydration shell) and enhance Tau condensation through hydrophobic interactions. Additionally, non-polar residues can favorably interact with each other and can give rise to precipitation of Tau and formation of amorphous structures instead of liquid droplet. Inevitably, any PTM of Tau can alter the strength of its inter- and intramolecular electrostatic and/or hydrophobic interactions. For example, PTM of a lysine residue such as acetylation not only neutralizes a positive charge, but also exposes its extended side chain, which now functions as a hydrophobic group facilitating dehydration.[3] The structural disorder, the multiplex cellular interactions, and tight cellular regulations together point to pleiotropic functions of Tau in cells.

Even though Tau can engage in myriads of interactions, the Tau-microtubule association is the dominant one and the estimated intracellular concentration of unbound Tau is low, reportedly below 10 nM.[22,23] This makes the advent of intracellular aggregation of Tau more puzzling as it necessarily requires higher local Tau concentration than the basal level in the normal cellular state. It is in this context that the emergence of Tau liquid–liquid phase separation (LLPS) into sub-cellular scale condensates has received enormous interest and generated new hypotheses in the research community of Tau biology.[4,8,13,24–31] It is an active debate whether LLPS promotes or protects from, or is not directly connected to pathological aggregation of Tau. The protein

concentration is increased in these fluidic biological condensates well above basal levels for Tau in the cell,[32,33] but the dynamics of Tau is also more limited, and hence the consequences of LLPS on the fibrilization propensity of Tau are not obvious.

The cellular factors that trigger and drive the LLPS of Tau are not known. In vitro, Tau readily undergoes complex coacervation with RNA and other polyanions driven by electrostatic interactions between them.[12,34] Interestingly, the positively charged lysine residues of Tau play important roles in the incorporation of Tau into stress granules that include RNA.[13] The N-terminal Tau and C-terminal Tau isoforms that harbor opposite net charges can undergo complex coacervation.[27] Hyperphosphorylated Tau, on the other hand, can readily undergo LLPS by self-coacervation (SC), especially when facilitated by depletion forces imposed by molecular crowding.[26] Interestingly, Tau without any modification can still undergo LLPS by SC when subjected to high NaCl concentration on the order of 2.5 M (or higher) that induces dehydration and hydrophobic association of Tau.[29] Taken together, we understand that LLPS of Tau can be driven by a combination of interactions mediated by electrostatic, hydrophobic and depletion forces.[13,24,26] Thus, the diversity of interactions that Tau can engage in under biological conditions is vast, given the myriad of PTMs that Tau can adopt. Fascinatingly, Tau can form liquid condensates at much lower basal levels of Tau in the presence of biomolecular constituents that strongly bind Tau and can engage in multivalent interactions.[28] Polyanions, in particular heparin, readily associates with Tau and promotes the liquid condensation of Tau, but also concurrently promotes aggregation.[29]

In this study we focus on comparing the factors that drive and facilitate the LLPS of Tau with itself (SC) and by complexation with other biomolecules (complex-coacervation [CC]). The experimental design is to choose a minimal system of Tau stripped of biological complexity to investigate the effect of the presence and absence of a heterotypic binding partner to Tau, here RNA, on the property of the liquid condensate. The questions are whether the SC (homotypic) versus CC (heterotypic) condensation have overlapping formation conditions, and how Tau chooses to adopt one or the other form of condensate. Inspiration for these questions comes from our recent study showing that the polyproline-rich region of Tau can drive LLPS in the cell, while at the same time Tau associates with EB1 to form condensates, shifting Tau from the GDP-gated microtubule lattice to the GTP-gated microtubule plus end.[30] When microtubules are depolymerized by nocodazole (a tubulin polymerization inhibitor), Tau's polyproline-rich region no longer

interacts with EB1, suggesting the balance is tipped towards potentially SC, or involves different heterotypic binding partners to Tau. The relative strength and interplay of the driving forces resulting from homotypic and different heterotypic interactions can significantly shift the phase diagram, that is, conditions, for LLPS. In this study, we demonstrate that Tau liquid condensates formed by SC and CC can coexist in solution over a range of biologically relevant conditions, and do not readily mix and interconvert to whichever LLPS state (SC or CC) is thermodynamically more favorable, suggesting that Tau homeostasis is a dynamic process, and the outcome can be kinetically driven subject to regulation by biological conditions.
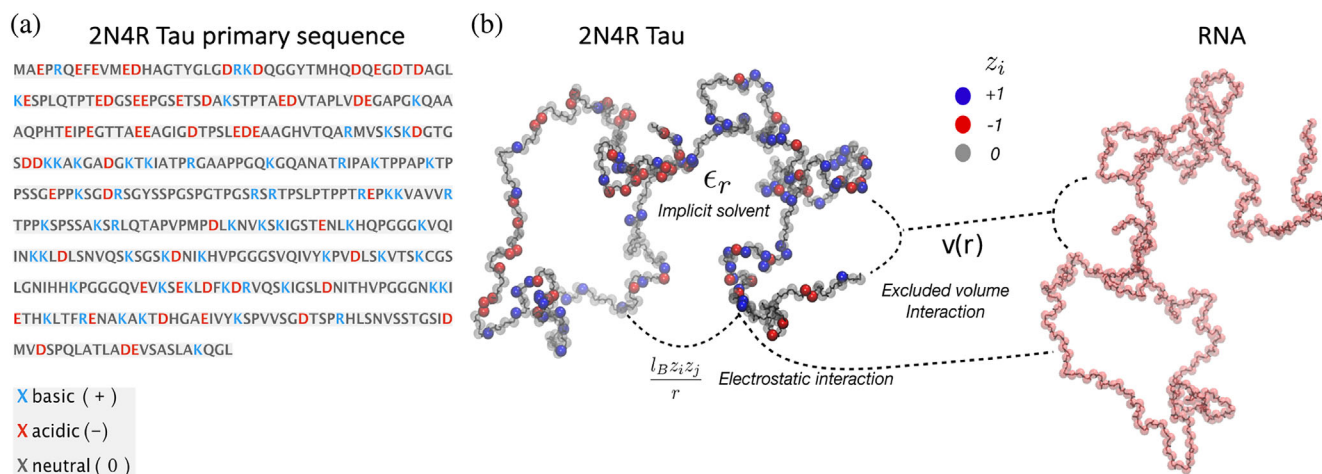
2 | RESULTS

2.1 | Tau undergoes electrostatically driven SC and CC

The question we pose is under what conditions does Tau undergo LLPS by itself versus upon complexation with RNA, and do the two coacervation mechanisms yield similar or different condensate properties? We pursue to answer this question using full-length human Tau 2N4R. To avoid potential interference due to disulfide bonding, we introduced C291S and C322S mutations, resulting in a cysteine-free pseudo wildtype construct, referred to henceforth simply as Tau. By assuming independent side chain ionization, the estimated net charge of Tau at neutral pH is +3.1 per Tau molecule, making it moderately positive (Figure 1a). Plotting the charge along the primary sequence shows that Tau can be considered a blocky polyampholyte with −19.6 charge from residues 1–150, which corresponds to the N terminal region, and +22.8 charge from residues 151–441 that includes the poly proline rich domain (PRD), the microtubule binding repeats R1-R4 and the C terminal region (Figure 1a). The primary sequence of 2N4R is shown in Figure 2a with the charge state, z_i, of each of the 441 residues
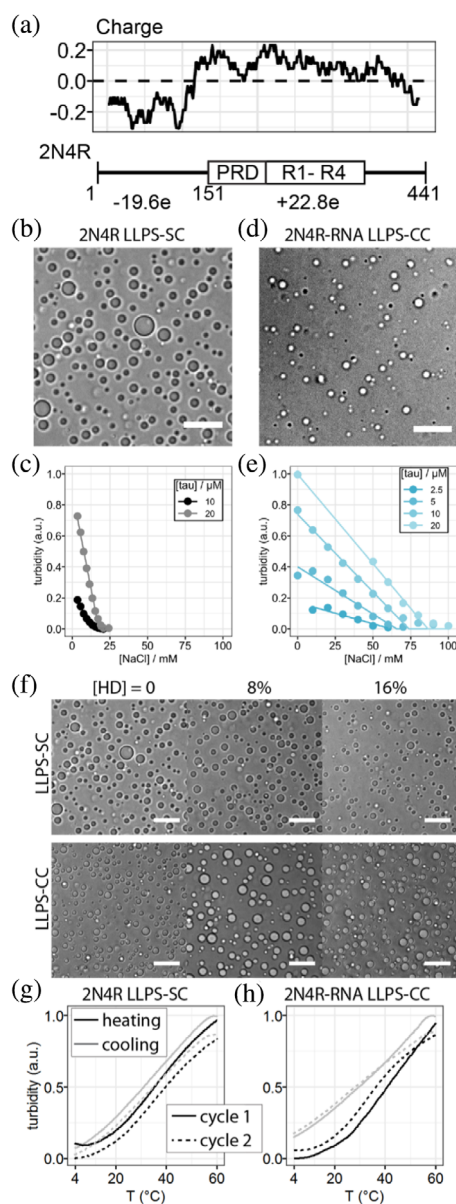
FIGURE 1 Bright field microscope images and turbidity of Tau LLPS-SC and LLPS-CC at varying conditions show that both types of processes are driven by electrostatic interactions and reversible. (a). Charge of 2N4R at pH 7.0. Data shows the moving average of consecutive 25 amino acid. (b). Representative bright field microscope image of full length 2N4R self-coacervate (LLPS-SC) at very low ionic strength (10 μM 2N4R and 5 mM NaCl). Scale bar length is 25 μm. (c). Turbidity of LLPS-SC samples with varying [Tau] and [NaCl]. (10 ~ 20 μM Tau, 5 ~ 25 mM NaCl were used) (d). Representative bright field microscope image of 2N4R-RNA complex-coacervate (LLPS-CC) at medium ionic strength (10 μM 2N4R, 20 μg/ml RNA and 40 mM NaCl). Scale bar length is 25 μm. (e). Turbidity of LLPS-CC samples with varying [Tau] and [NaCl] (2.5 ~ 20 μM Tau and 0 ~ 100 mM NaCl were used). The same [RNA]:[Tau] ratio was used (2 μg/ml RNA per 1 μM Tau). In both (c) and (e), solid lines show the fitted results using function y = max(0, a-bx), where a, b > 0. (f). Bright field microscope images of LLPS-SC and LLPS-CC at the same conditions as in (b) and (d), except with the addition of varying 1,6-hexanediol (HD) volume percentages. (g). Heating–cooling cycles of LLPS-SC formed by 20 μM 2N4R in presence of 3 mM NaCl. (h). Heating–cooling cycles of LLPS-CC formed by 20 μM 2N4R in the presence of 34 μg/ml RNA and 80 mM NaCl. In both (g) and (h), the turbidity readings were scaled to show the relative difference between different cycles. Figures (a) and (f) are reproduced from Figure 1 in reference [29] with permissions

(a)

2N4R Tau primary sequence

MAEPRQEFEVMEDHAGTYGLGDRKDQGGYTMHQDQEGDTDAGL
KESPLQTPTEDGSEEPGSETSDAKSTPTAEDVTAPLVDEGAPGKQAA
AQPHTEIPEGTTAEEAGIGDTPSLEDEAAGHVTQARMVSKSKDGTG
SDDKKAKGADGKTKIATPRGAAPPGQKGQANATRIPAKTPPAPKTP
PSSGEPPKSGDRSGYSSPGSPGTPGSRSRTPSLPTPPTREPKKVAVVR
TPPKSPSSAKSRLQTAPVPMPDLKNVKSKIGSTENLKHQPGGGKVQI
INKKLDLSNVQSKSGSKDNIKHVPGGGSVQIVYKPVDLSKVTSKCGS
LGNIHHKPGGGQVEVKSEKLDFKDRVQSKIGSLDNITHVPGGGNKKI
ETHKLTFRENAKAKTDHGAEIVYKSPVVSGDTSPRHLSNVSSTGSID
MVDSPQLATLADEVSASLAKQGL

X basic (+)
X acidic (−)
X neutral (0)

(b)

FIGURE 2 Model depiction of Tau and RNA. (a). The primary sequence of 2N4R Tau is shown with the C291 and C322 cysteines intact as in wild type. The basic ($z_i = +1$), acidic ($z_i = -1$) and neutral ($z_i = 0$) residues are shown in blue, red, and gray respectively. (b). A schematic illustration of the bead-spring model of Tau and RNA in implicit solvent with a homogenous dielectric constant of $\epsilon_r = 81$, representing water. The charge of each coarse-grained residue is assigned based on the amino acids net charge at pH = 7.0. RNA is modeled by a polyanion with uniform charge density per monomer ($z_i = -1$). In the coarse-grained model, the successive beads on the chain are connected via a simple harmonic potential. All monomers repel each other with a short-ranged Gaussian repulsive interaction, and charged beads interact through a long-ranged Coulomb potential

(i = 1–441) indicated with color coding. However, unlike in a polymeric diblock polyampholyte, each oppositely charged block of Tau is still interspersed by non-charged, hydrophobic and/or oppositely charged residues and has relatively low net charge density per block, while Tau adopts relatively extended conformation in solution state.

The resemblance of Tau to a net charge-matched diblock polyampholyte, albeit with low net charge density per block, suggests that the driving force for the SC of Tau can readily come from homotypic electrostatic interactions between oppositely charged domains of Tau.[35,36] To test this hypothesis, we subjected Tau dissolved in a solution with ionic strength of 100 mM to a solution of much lower ionic strength of below 5 mM to enhance the effective charge density of each charged block of Tau. Immediately upon dropping the ionic strength of the solution, the clear solution of Tau became turbid and droplets appeared (Figure 1b), indicating LLPS by SC (LLPS-SC). Notably, LLPS-SC occurred without adding molecular crowding reagents and using Tau free of PTMs, indicating that the interactions among Tau and water molecules are sufficient to drive LLPS-SC. Turbidity (measurement of absorbance at $\lambda = 500$ nm) has been shown to linearly correlate with the volume fraction of the dense phase of polyelectrolyte coacervates.[28] By plotting turbidity as a function of [NaCl], we observe that the dense phase of LLPS-SC monotonically and steeply reduces with increasing [NaCl], and is eliminated at and above [NaCl] = 25 mM (Figure 1c). This result shows that electrostatic interactions are essential to

LLPS-SC. Titrating LLPS-SC with increasing amounts of 1,6-hexanediol (1,6-HD) showed no distinguishable decrease in droplet amounts according to bright field microscopy images (Figure 1f). The 1,6-HD has been shown to dissolve LLPS formed by hydrophobic association of proteins, prevalently under cellular conditions.[26,37–39] The insensitivity to 1,6-HD found for LLPS-SC of Tau suggests that its formation does not rely on hydrophobic interactions, but rather on electrostatic interactions to form hydrophilic condensates.[29,37]

The estimated moderately positive net charge of +3.1 per Tau molecule at neutral pH suggests that Tau can undergo CC upon complexation with the polyanion RNA. Since 2N4R Tau has an average charge density of +0.068 e/kD and the PolyU RNA (Sigma P9528) we used has a charge density of −3.2 e/kD, we mixed Tau with RNA at a wide range of RNA:Tau charge ratios, including charge matching conditions of 1:1 (corresponding to mass ratio RNA:Tau of 1:50). In order to drive Tau towards LLPS-CC and initially suppress LLPS-SC, we mixed Tau with RNA in the presence of [NaCl] = 40 mM. Immediately upon mixing Tau and RNA at a charge matching ratio, an abundant number of microscopic liquid droplets become visible (Figure 1d). By varying the ratio of RNA:Tau, we observe according to the turbidity readings that the abundance of LLPS peaks at a charge ratio of ~2:1 and that LLPS is clearly detected at charge ratios ranging from 0.5:1 to 4:1 (Figure S1). This finding of LLPS at charge ratios not too far from where net charge neutrality is expected suggests that LLPS favorably form under

charge-balancing conditions. The deviation of the optimum condition from the charge matching condition of 1:1 likely originates from the fact that the RNA chain is ~10 times longer and has ~50 times higher charge density compared to Tau, so that not all charged moieties of RNA are simultaneously displayed and able to interact with the more sparsely distributed positively charged side chains of Tau. This explanation would be consistent with needing a larger concentration of RNA to effectively achieve charge neutrality for association with Tau. Similar to LLPS-SC, the amount of the LLPS-CC dense phase is reduced with increasing [NaCl] and is eliminated at and above [NaCl] ≈ 80 mM (Figure 1e). This is similar to the observation for LLPS-SC shown in Figure 1c, implying that both LLPS-SC and LLPS-CC of Tau rely on electrostatic interactions. Adding 1,6-HD up to 16% induces no visible reduction of the droplet amounts, confirming that either type of LLPS has a hydrophilic core (Figure 1f).

Tau-RNA CC has been shown in a previous study to be an equilibrated state, and that its formation is reversible.[12,28] Here we test whether both Tau LLPS-CC and LLPS-SC formation is reversible. We prepared LLPS-SC and LLPS-CC samples at the same concentration of Tau and subjected the samples to consecutive heating and cooling cycles. Turbidity results showed that both SC and CC formation are favored at higher temperature (Figure 1g, h) following lower critical solution temperature (LCST) behavior, suggesting that both forms of LLPS are entropy driven. Consecutive heating–cooling cycles showed that the droplet amount at low and high temperature states as measured by turbidity, as well as the transition temperature where droplets start to occur or dissolve are invariant (Figure 1g, h). Hence, the formation is reversible for both types of LLPS. ThT fluorescence assays showed that Tau LLPS-SC and Tau-RNA LLPS-CC are free of detectable amyloid aggregates in the experimental time span (in contrast to Tau-heparin LLPS that shows robust ThT readings, see Figure S2). Using site-directed spin labeling and Double Electron Electron Resonance (DEER), we measured the probability distribution P(r) of the intra-molecular distance between site 300 and site 313 of Tau of the full ensemble of Tau in the solution. The distribution of distances spanning sites 300 and 313 report on the ensemble conformational property of the segment spanning the aggregation hotspot [306]VQIVYK[311].[1,40,41] The shape of P(r) of the ensemble of distance, r, spanning the two sites 300 and 313 appears indistinguishable for Tau in the LLPS-SC or LLPS-CC state relative to Tau in dilute solution (Figure S3). This observation suggests that Tau overall retains solution state conformations in the aggregate-free liquid condensed phase.

The findings show a highly similar formation mechanism for Tau LLPS-SC and LLPS-CC driven by electrostatic interaction, under distinct, but still overlapping, conditions for the LLPS by SC and CC of Tau. Tau is able to undergo both SC and CC in the range [NaCl] = 0 to 20 mM. The LLPS-CC is stable under a broader range of conditions of [NaCl] = 0 to 100 mM for the tested system and conditions. However, it is unclear whether this reflects on a general property of the LLPS of Tau formed by homotypic vs heterotypic interactions, and if so, what are their driving factors. We turn to the computation of the full phase diagram of the LLPS-SC and CC by field-theoretic simulations to address this question. The computational study allows us to examine the interaction type and strength underlying LLPS by SC of Tau and CC of Tau-RNA, as well as the extent of overlap or difference in their phase diagrams.

2.2 | Tau phase behavior with and without RNA

To understand the principle and governing interactions driving Tau LLPS-SC and Tau-RNA LLPS-CC, we constructed the theoretical phase diagram by performing Field-Theoretic simulations via Complex-Langevin sampling (FTS-CL).[35,42–47] We employ a coarse-grained (CG) discrete Gaussian chain[48,49] (DGC) model to describe Tau as a linear collection of bonded monomers through a simple harmonic potential; each residue of Tau is represented by a monomeric unit with diameter $b \tilde{3}.8$Å (featuring the distance between successive C_α atoms along Tau polypeptide). The monomers experience a short-range Gaussian excluded volume potential, as well as a long-range electrostatic Coulomb potential mediated by a uniform dielectric constant. In the DGC model, the charge of each residue is embedded in units of elementary charge e according to the charge pattern of the primary amino acid sequence of Tau, as illustrated in Figure 2a. The same DGC polymer model describes RNA as a polyanion with a uniform charge distribution; the polyanion consists of 441 monomeric units with diameter b and charge density $z = -1$.

In Figure 2b, a schematic view of full-length Tau and RNA with the underlying model force field is shown; the red, blue and gray monomers represent residues with negative, positive and neutral charges, respectively. In this CG polymer model, the solvent and its quality are treated implicitly by the strength of the Gaussian excluded volume potential. Under good solvent conditions, the polymer adopts extended conformations resulting from the dominant hydrophilic interactions between the polymer and water molecules, while in a

poor solvent near the theta-condition the polymer tends to collapse and feature pseudo-globular states.[48,49] In an implicit solvent model, good versus poor solvent quality can be represented by a strong versus weak excluded volume interaction between the monomeric units of the polymer, respectively. The strength of the excluded volume potential is characterized by the v parameter that scales with the cube of the monomer's diameter, $v \propto b^3$. The strength of the electrostatic interaction and its temperature dependence is encoded in a dimensionless characteristic length known as the Bjerrum length $l_B = \frac{e^2}{4\pi\epsilon_0\epsilon_r k_B T}$, where ϵ_0 and ϵ_r are the vacuum permittivity and the solvent dielectric constant, respectively. The electrostatic interaction between charged monomers can be affected by the thermal fluctuation energy ($\sim k_B T$) when the molecular distance is of the order of l_B (under physiological conditions at T = 300 K the Bjerrum length of water is $l_B = 7.1$ Å). In general, salt in solution can diminish the electrostatic interaction by screening the potential created by the bound charges. Hence, in an implicit solvent model, the effect of salt can be approximately accounted for by tuning the Bjerrum length; specifically, l_B is proportional to the inverse salt concentration. In this study, the counterions of Tau are modeled explicitly by the aforementioned monomeric units with charge valence $z = -1$.

Using the CG polymer model that encodes the charge-based electrostatic interactions of Tau and RNA in an implicit solvent, we employ FTS-CL to obtain phase boundaries of Tau SC and Tau-RNA CC. It is known that due to the hydrophobicity enhancement of Tau as the result of temperature increment, Tau can exhibit lower critical solution temperature (LCST) in a semi-infinite macroscopic system, in which Tau LLPS can be affected by hydrophobic and other short-range electrostatic interactions such as cation-π and π-π interactions. In this study, for the sake of characterizing the effect of RNA on Tau phase behavior we have simplified our polymer model to account for the long-range electrostatic interaction and its interplay with the thermal fluctuation that is sufficient to effectively trigger Tau condensation.[28] The counterions and RNA concentrations are regulated to satisfy the charge balancing condition of Tau SC and Tau-RNA CC, respectively. We fix the strength of the excluded volume interaction near a good solvent condition as $v = 0.03$ b^3 and vary the Bjerrum length l_B (which models the variation in [NaCl]$^{-1}$) to construct the full phase diagrams of Tau SC and CC. Given the known intrinsically disordered nature of Tau in solution state, the choice of a good solvent condition as represented by an empirical value $v = 0.03$ b^3 that gives rise to relatively extended Tau conformations is a reasonable approximation.[50]

First, to reveal the effect of electrostatic interactions on Tau LLPS-SC, we perform FTS-CL using a small ($l_B = 0.12$ b) and a large ($l_B = 1.2$ b) Bjerrum length at a fixed total Tau concentration ($\rho b^3 = 0.01$), representing weak and strong electrostatic interaction, respectively. In Figure 3a, we illustrate a FTS-CL snapshot of Tau density in the weak electrostatic interaction strength (low [NaCl]$^{-1}$) solution state, wherein Tau proteins are uniformly distributed throughout the entire simulation box without featuring a dense coacervate phase. However, by increasing the strength of the electrostatic interaction to $l_B = 1.2$ b (high [NaCl]$^{-1}$), as illustrated by an instantaneous FTS-CL snapshot in Figure 3b, Tau chains undergo LLPS-SC, in which the dense coacervate phase (red) is in coexistence with the surrounding dilute solution (white) of Tau. As elucidated in Figure 3, FTS-CL can be employed to determine the phase behavior of Tau under different thermodynamic conditions (as featured by l_B) and can then be used to rigorously construct the full-phase diagram. The binodal phase boundaries for a given l_B can be obtained by performing several FTS-CL simulations under varying Tau concentration to locate the concentrations of Tau monomers (ρb^3) in the dilute and dense phases at coexistence (in which the chemical potentials and osmotic pressures of the two-phases are equal, with further technical details described in the SI). To construct the full phase diagram, we repeat this procedure for the range of desired l_B values and determine the binodal phase boundaries. In Figure 4a, we show the phase diagrams of Tau LLPS-SC and Tau-RNA LLPS-CC obtained from FTS-CL in the space spanned by the Bjerrum length l_B and the dimensionless Tau concentration ρb^3. As illustrated in Figure 4a, increasing l_B (or the reduction of charge screening effect) promotes the attractive electrostatic interaction between oppositely charged residues of Tau and enhances the driving force of LLPS, leading to an expansion of the phase envelope in which the Tau dense phase is stable, and coexists with the surrounding Tau dilute region. Comparison of the phase boundaries of the two types of LLPS indicate that the general trend of LLPS-SC and LLPS-CC is similar, but that Tau-RNA CC has a broader two-phase region than Tau SC, suggesting that the presence of RNA increases the driving force of LLPS and hence promotes Tau coacervation. Notably, under conditions resembling the cellular environment (which corresponds to l_B values between 1.6 b − 1.75 b, depending on the salt concentration and temperature), the driving force to form Tau-RNA CC is distinctly greater than Tau SC. This phase region is highlighted in the inset plot of Figure 4a. The theoretical phase diagrams studies reveal that the presence of RNA triggers Tau condensation with higher propensity than Tau SC. This observation that the set intermolecular

FIGURE 3 Tau density distribution in single-phase solution and coacervate phase resulted from FTS-CL. (a). Tau proteins are uniformly distributed throughout the simulation box in weak electrostatic interaction $l_B = 0.12\ b$. (b). Under strong electrostatic interaction $l_B = 1.2\ b$, Tau undergoes SC. The color code from blue-white-red indicates the increment of local Tau density. Note that in both systems the Tau concentration is fixed at $\rho b^3 = 0.01$ and the excluded volume interaction strength is set near a good solvent condition $v = 0.03\ b^3$
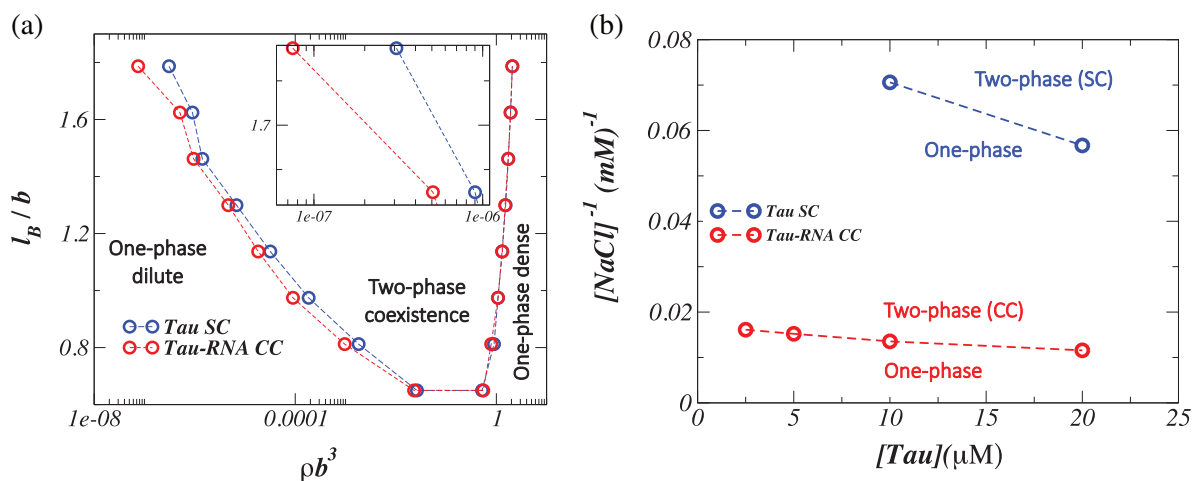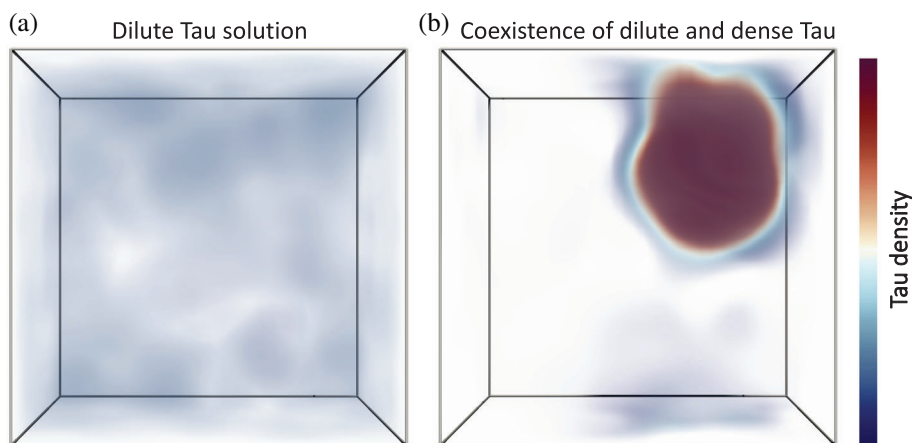
FIGURE 4 Phase behavior of Tau and Tau-RNA. (a). the binodal phase boundaries of Tau SC (blue) and Tau-RNA CC (red) as a function of Bjerrum length l_B and dimensionless Tau concentration ρb^3 calculated from FTS-CL near a good solvent condition at $v = 0.03\ b^3$. (b). The dilute branch of Tau SC and Tau-RNA CC phase boundaries obtained from *in vitro* experiment

interactions within the condensates are different is consistent with the dissimilarities that we observe between the liquid properties of the Tau SC and Tau-RNA CC droplets, to be discussed in the next section.

We also acquired the experimental binodal phase diagram for both Tau LLPS-SC and LLPS-CC, as shown and overlaid in Figure 4b. It is evident from the outlines of the phase boundaries that with increasing $[NaCl]^{-1}$ (decreasing charge screening) the phase region widens and stabilizes the coexistence of the dilute and dense phases, such that even at very low Tau concentration in solution, coacervation occurs spontaneously. Furthermore, Tau LLPS-CC features a much broader phase region than that of Tau LLPS-SC, which clearly indicates that Tau-RNA condensation can readily occur at much lower $[NaCl]^{-1}$ (higher salt screening) than LLPS-SC. Hence, the experimental trends are in qualitative agreement with that found in the theoretical FTS-CL phase diagrams. We can conclude that the thermodynamic

propensity for Tau to undergo LLPS-CC upon complexation with RNA is greater than LLPS-SC, implying that the driving forces for Tau-RNA CC is larger than for Tau SC.

Though the phase diagram studies have clearly indicated that electrostatic interactions are the key driving forces for Tau LLPS-SC and Tau-RNA LLPS-CC, it is rather challenging to dissect the exact underlying molecular interactions. We speculate that in the CC process, RNA enhances Tau phase separation through a heterogeneous mechanism, in which RNA associates with multiple Tau molecules to localize Tau. Both the theoretical FTS-CL and experimental phase diagrams reveal that under physiological conditions, full-length 2N4R Tau can readily and reversibly undergo LLPS by SC and CC, driven by homotypic or heterotypic electrostatic interactions with no obvious difference in the mechanism of phase separation other than the strength of the interaction.

2.3 | Tau SC and CC condensates stability

Next, we investigate the viscosity of the dense condensed phase of Tau upon LLPS. We focus on studying the emergent properties of the Tau liquid condensates by employing micro-viscosity-sensitive molecular rotors,[51–53] specifically the fluorescent boron-dipyrromethene (BODIPY) containing an NHS-ester moiety.[51] Fluorescent lifetime imaging measurements (FLIM) were performed for both LLPS-SC and LLPS-CC droplets using NHS-ester functionalized BODIPY tethered to Tau. The fluorescent lifetime of these dyes in solution displays a power law relationship with the micro-viscosity in a limited range spanning 0 to ~5,000 cP, described by the Förster-Hoffmann equation.[52] Low fluorescent lifetimes represent fluid, water-like environments and high lifetimes more viscous, solid-like properties. Factors that can influence the local micro-environment of the system include various intermolecular interactions that, in turn, depend on protein structural, topological and conformational

properties. When comparing the lifetimes of BODIPY linked to Tau in the dense phase of SC and CC, the micro-viscosity in the Tau-RNA CC droplets is clearly much higher than in the Tau SC droplets (Figure 5). The fluorescence lifetime of Tau-tethered BODIPY was 3,700 ps (310 cP) in Tau SC and 4,400 ps (2,100 cP) in Tau-RNA CC, representing a ~ 7-fold difference in the droplet-internal micro-viscosity. This observation supports the previous finding by FTS-CL and experiments (Figure 4) that Tau-RNA interactions are stronger than Tau-Tau interactions. The higher micro-viscosity in the Tau-RNA CC droplets may also be contributed by greater physical entanglement between Tau and RNA, with RNA possessing larger molecular weights. In either case, there must be multivalent interactions between Tau-RNA and Tau-Tau constituents that enhance a network of interactions.[54]

Interestingly, both the SC and CC droplets feature a significant relaxation in the micro-viscosity over the course of 24 h, dropping from 3,700 ps (310 cP) to 3,100 ps (40 cP) in SC, and 4,400 ps (2,100 cP) to 3,700 ps
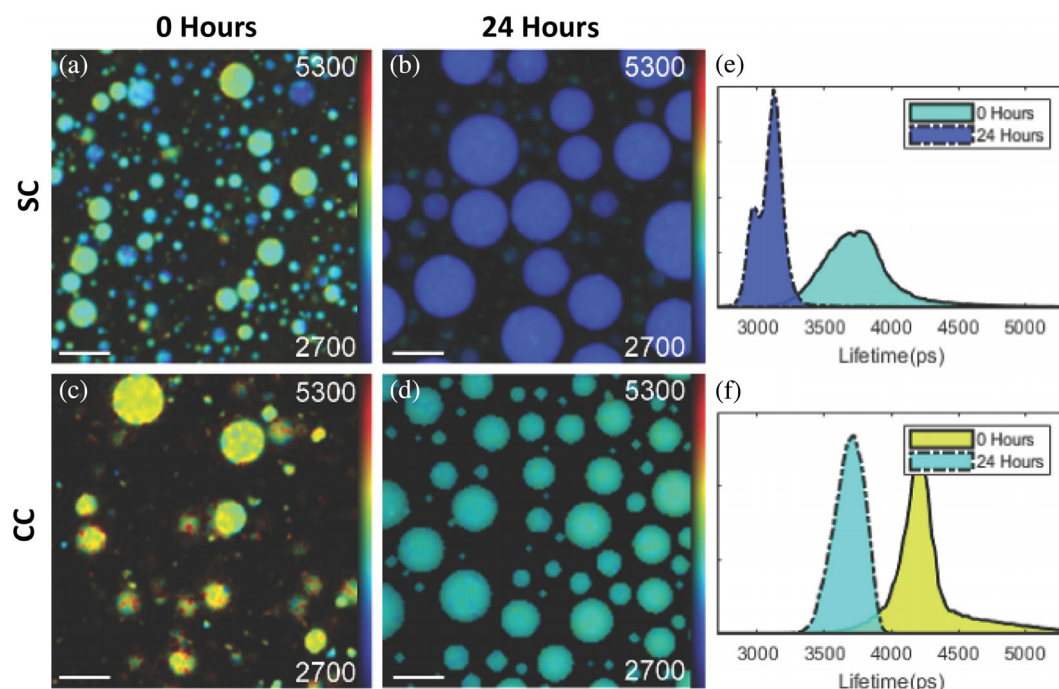

FIGURE 5 FLIM of Tau LLPS-SC and Tau-RNA LLPS-CC. Fluorescence Lifetime Imaging Measurements (FLIM), were taken at 0 and 24 h at the same resolution, scale bar 25 μm. (a-d), Fluorescent microscope images of Tau-RNA droplets and Tau LLPS droplets before (0 h) and after incubation (24 h). Individual pixels were fit with a 2 component exponential decay using the FLIMfit software tool developed at Imperial College London, and the data was visualized using the higher lifetime component. The colors in the fluorescent images and corresponding histograms represent a pseudo-color heat map that ranges from 2,700 to 5,300 ps, with blue representing low lifetimes and red representing high lifetimes. (e), and (f), Histograms of fitted results in of SC and CC respectively. The histograms are normalized so that area under the curve is 1. The color under each histogram corresponds to the pseudo-color of the heat map at the histograms max value. Solid line = 0 h, Dashed line = 24 h. (e). Histogram of SC showing the relaxation of the micro-viscosity from 3,700 ps to 3,100 ps over the course of 24 h. (f). Histogram of CC showing the relaxation of the micro-viscosity from 4,400 ps to 3,700 ps over the course of 24 h. (Figure (c), (d), (f) have been adapted from reference [29] with permission)

(310 cP) in CC droplets. Interestingly, this drop in viscosity is accompanied by a distinct increase in droplet size over time (Figure 5a–e), presumably due to Ostwald ripening and droplet coalescence that occurs more readily between low viscosity droplets. Recent studies described aging in biological droplets being dominated by changes in the droplet viscosity, as opposed to elasticity.[55] The significant and systematic drop in droplet micro-viscosity implies that the intramolecular and/or intermolecular interactions of Tau are changing over time. Notably, both systems show a comparable seven-fold change in micro-viscosity over the course of 24 h, implying that similar mechanisms are at play, and that the timescale for the molecular rearrangements of Tau accompanied by the drop in micro-viscosity is comparable. These results suggest that the conformational and/or interaction state of Tau must be different in the liquid condensed phase of SC vs CC upon formation, as well as evolves with time. However, DEER-derived intra-Tau distribution P(r) of distance r between sites 300–313 of the ensemble of Tau is found to be indistinguishable in the dense LLPS state of SC versus CC. Possibly, the P(r) of the particular R3 MTB segment (see Figure 1) spanned by sites 300 and 313 of Tau is insensitive to the conformational change adopted by Tau in the different liquid droplet phase over time. What is clear is that the CC droplets stay consistently more viscous than the SC droplets (Figure 5e, f). We can currently only speculate about the molecular basis and biological implication of this fascinating observation. Liquid condensates that become less viscous over time promote exchange of their constituents and may be more readily reversible. We next focus on the role of RNA in stabilizing CC droplets, presumably by a network of Tau-RNA associations held together by multivalent Tau-RNA interactions.

The experimental study of micro-viscosity is complemented by Molecular Dynamics (MD) investigation of the thermomechanical properties of the SC and CC droplets. Within coacervates, charged species engage in electrostatic associations that continuously form and break with certain rates, and cause the droplets to manifest viscous features. The time scale and strength of the inter- and intramolecular electrostatic interactions contribute directly to the viscosity of the droplets and their thermomechanical stability. Here, in order to overcome the slow kinetics of droplet formation in MD simulations, we initiated Tau condensation by slowly dragging all the chains to the center of the simulation box to create a locally Tau rich region; a similar approach of seeding LLPS of a dense IDP slab domain has been used previously for the study of LLPS by MD simulations.[56,57] To examine the thermomechanical stability, we increased the temperature of the well-equilibrated preformed

droplets above a threshold value in which the *quasi-static* condensate starts to unravel, and so increase the Tau concentration in the surrounding dilute phase in a finite MD simulation box. We employ the Kremer-Grest polymer model in an implicit solvent,[58] to treat Tau as a linear collection of coarse-grained (CG) monomeric units, such that each monomer represents an amino acid that its charge is embedded in the unit of the elementary charge e based on the Tau primary sequence. In this polymer model, the successive monomers with diameter $b = 3.8\,\text{Å}$, are connected through a finite extensible nonlinear elastic (FENE) potential and prevented from volume crossing by applying a Weeks-Chandler-Andersen (WCA) excluded volume potential (See the SI). Additionally, the charged monomers interact through long-ranged Coulombic potential in a fixed background dielectric constant $\epsilon_r = 81$. RNA is modeled as a polyanion with uniform charge density per monomer ($z = -1$) by using the same Kremer-Grest polymer model. The counterions are represented by single charged monomers that interact through long-ranged Coulombic interaction and also exclude other monomers via the WCA potential. Here, the Tau droplet consists of 48 Tau chains, and the Tau-RNA CC droplet in addition to 48 Tau chains includes 10 short RNA fragments (with 10 monomers length).

Using this CG polymer model, we gain insight into the thermomechanical properties of the Tau SC and Tau-RNA CC condensates by characterizing the number of Tau chains in the largest droplet present in the simulation box at different temperatures. The size of the SC and CC droplets as a collective variable can reveal the strength of the molecular interactions that directly contribute to droplet stability. As shown in the MD simulation snapshots of the Tau SC and Tau-RNA CC droplets in Figure 6a,b, respectively, at temperature $T = 0.5$ (in LJ units) the Tau-RNA droplet is larger and contains a greater number of Tau chains within the condensate. The thermomechanical stability between the Tau SC and Tau-RNA CC droplets is further compared at higher temperatures, as shown in Figure 6c. The size of both the SC and CC droplets decreases with increasing temperature. Interestingly, the size of the SC droplet diminishes faster than of the Tau-RNA droplet. At temperature $T = 0.8$, the SC droplet has completely dissolved, while under the same thermodynamic condition the Tau-RNA CC droplet only breaks down to multiple mini-droplets in which RNA fragments are wrapped by Tau chains (See SI, Movie 1). These results show that even at higher temperature, RNA can effectively engage in intermolecular electrostatic interactions with Tau. Note that in this simple polymer model, effects of the changing solvent quality and H-bonding characteristics of water as a function of temperature are not included. Therefore, the
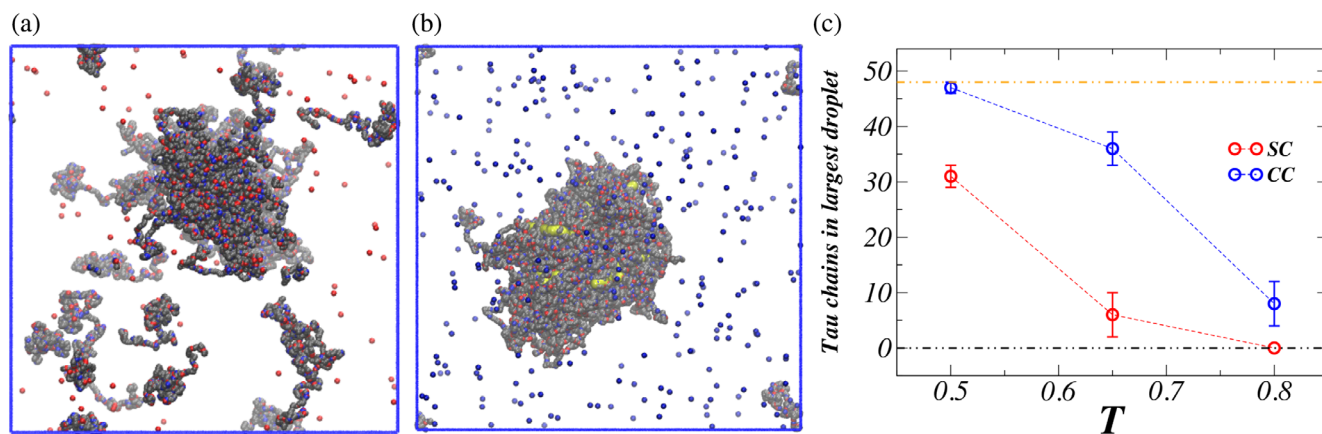
FIGURE 6   The thermomechanical stability of Tau and Tau-RNA droplets. In panel (a) and (b), we show the representative snapshots of the molecular dynamics (MD) simulations of the Tau SC and Tau-RNA CC droplets. The basic, acidic, and neutral residues are shown in blue, red, and gray respectively. In (b), the buried RNA fragments are colored in yellow. (c), The number of Tau chains within the SC and CC droplets as a function of temperature obtained from MD simulations

thermomechanical behavior of droplets only characterizes the strength of the electrostatic interactions between the polymer constituents within the Tau condensates.

Clearly, Tau can readily form liquid condensates with other Tau or RNA molecules to form SC or CC droplets under a range of conditions, while Tau-RNA molecules effectively engage in multivalent interactions. This prompts the question about the competition for free Tau between the SC and CC droplets that have different viscous properties. When we choose conditions common for the formation of SC or CC droplets, in the presence of RNA, will Tau choose to partition into SC or CC droplets? To answer this question, we next explore experimental conditions that allow us to systematically and selectively shift the thermodynamic propensity favoring CC versus SC droplets.

2.4 | Coexistence of Tau SC and CC condensates

The experimental and computational phase diagrams revealed that overlapping condition for the occurrence of Tau SC and Tau-RNA CC is relatively narrow (see the inset of Figure 4a). In cellular environments, LLPS of Tau is directly impacted by the presence of biomolecular binding partners to Tau that can engage in multivalent homotypic and heterotypic interactions. Non-binding macromolecules can also influence the LLPS of Tau if they enhance the excluded volume interactions among Tau and its binding partners and/or promote the dehydration of Tau that enhances hydrophobic Tau-Tau interactions. Here, we examined the factors that can utilize these effects to regulate the balance between SC and CC.

For the purpose of systematically enhancing Tau LLPS by CC, RNA concentration is the obvious tuning variable. The [NaCl] cannot be used as a variable to selectively enhance SC or CC as it affects both forms of droplets. Instead, we test the effect of a model molecular crowding agent PEG to control Tau LLPS by SC, inspired by prior studies.[59] PEG promotes LLPS through entropy-driven depletion interactions, largely enhanced by dehydration.[59] By varying PEG concentration, we found an experimental state in which the Tau SC and Tau-RNA CC droplets are in coexistence in a solution of 20 μM 2N4R, 40 μg/ml RNA and 8% PEG at room temperature (Figure 7a). To distinguish between CC and SC, RNA was labeled with tetramethylrhodamine (TAMRA) which fluoresces in red. The results show an abundance of both red bright droplets and transparent droplets, indicating the presence of both RNA-containing and RNA-free droplets, representing Tau SC and Tau-RNA CC, respectively. Interestingly, we observe that the droplets are either fully bright red, or completely transparent and fluorescence-free. The observation of apparent immiscibility of Tau SC droplets and Tau-RNA CC droplets raises the question: what factors determine the partitioning of Tau in SC or CC droplets? To characterize the role of PEG and RNA on Tau LLPS, we fix the crowding agent concentration at 8% PEG and then systematically increase the concentration of RNA from 0 to 80 μg/ml. When increasing the amount of RNA into the saturated solution of Tau, we observe that the volume fraction of fluorescent/RNA-containing Tau-RNA CC droplets systematically increases, as shown in Figure 7b. Conversely, when we fix the RNA concentration at 20 μg/ml and increase PEG concentration from 0 to 16%, we observe that this time the fraction of
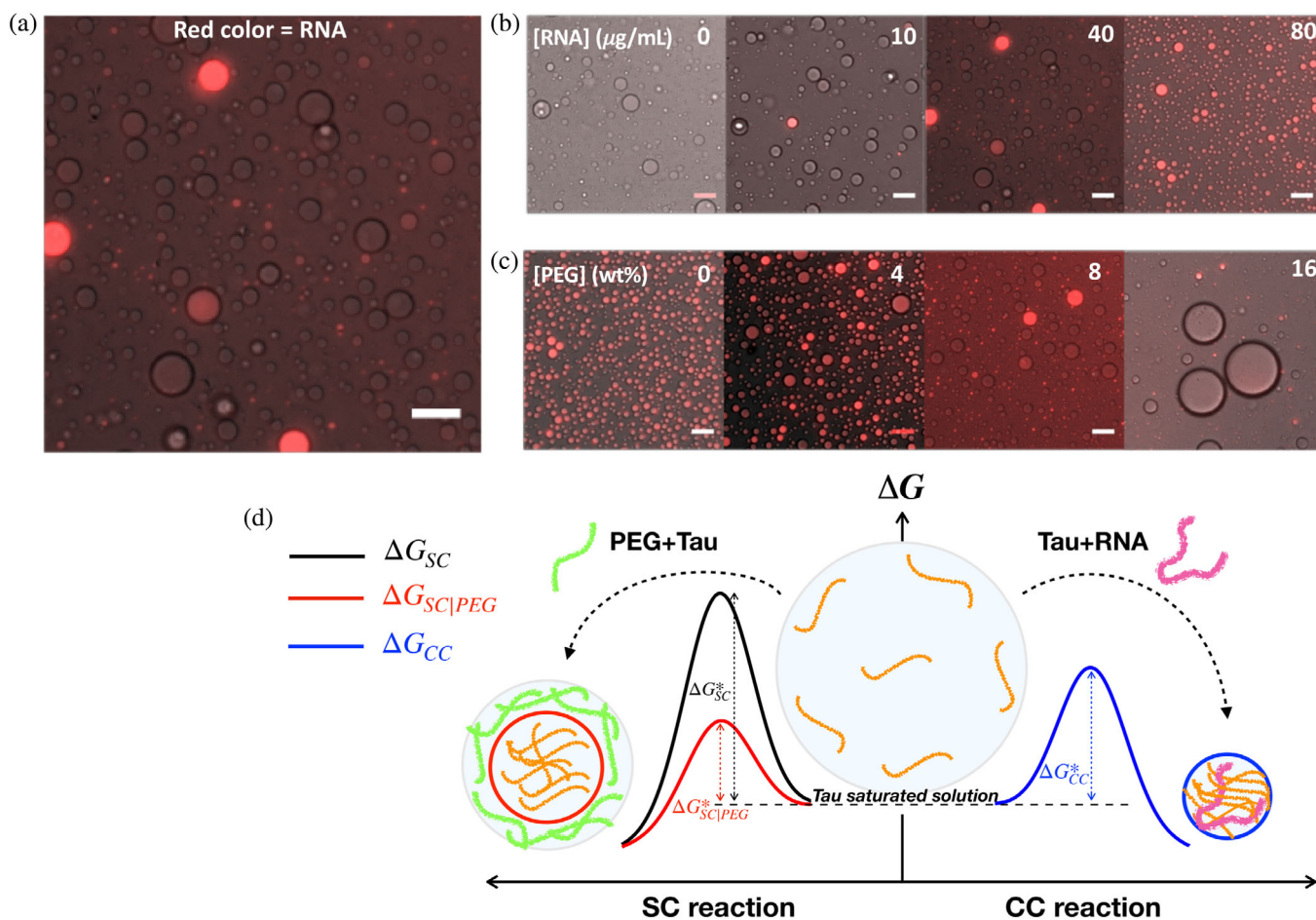
FIGURE 7 Coexisting of Tau SC and Tau-RNA CC. (a). Competition of SC-LLPS and CC-LLPS. 20 µM 2N4R, 40 µg/ml RNA and 8% PEG (20 kDa polydisperse [Sigma]) were used. (b). Effects of RNA on conversion of SC to CC. 8% PEG was used. (c). Effects of PEG on conversion of CC to SC. 20 µg/ml RNA was used. In both b and c, 20 µM 2N4R Tau was used. Scale bar lengths are all 25 µm. (d). A schematic free-energetic representation of Tau SC and CC competition

fluorescence-free/RNA-free Tau SC droplets increases and dominates with increasing PEG concentration, as shown in Figure 7c. In other words, even in the presence of RNA, Tau selectively partitions into SC droplets under conditions of high crowding pressure. The results show that the fraction of Tau SC and Tau-RNA CC droplets can be deliberately and separately regulated by tuning the concentration of PEG or RNA, respectively. What is the LLPS mechanism that would lead to Tau choosing to partition into either SC or CC droplets that, once formed, apparently do not mix and interconvert?

Both the SC and CC processes may be associated with a significant activation barrier, requiring the formation of a nucleus in solution to be kinetically viable. PEG as a molecular crowding agent may lower the threshold of nucleating the association of Tau into clusters or small droplets. Alternatively, analogous to a heterogeneous nucleation mechanism, RNA molecules may directly engage with Tau proteins through electrostatic interactions to form a nucleus, again in the form of a cluster or small droplets. Here, a cluster is referring to the assembly of a few to tens of Tau molecules, while a droplet contains many more Tau molecules that form a condensate. The addition of PEG enhances Tau SC by reducing the energetic barrier to trigger nucleation, while the reverse process for Tau CC to dissolve into its solution constituents is unfavorable given that it is uphill and there is no factor that lowers the barrier for dissolving Tau CC droplet. Similarly, if the addition of RNA enhances Tau CC by reducing the activation energetic barrier for nucleating the formation of Tau-RNA clusters or droplets, then the reverse process of dissolving Tau SC is unfavorable, given that the conditions may not lower the energy barrier for dissolving Tau SC droplets, hence hindering Tau SC droplets from converting to Tau CC droplets. This idea is schematically summarized in Figure 7d. The size of the nucleus and any additional microscopic details of a Tau nucleation process is entirely

unknown, and hence calculation of the rates of SC or CC in a given thermodynamic condition is elusive. We suggest that, in the presence of PEG or RNA, the SC or CC formation is in the binodal phase region and hence experience a kinetic barrier that are proportional to $\exp\left(-\Delta G_i^* / k_B T\right)$, where ΔG_i^* is the free energetic barrier of Tau nucleation (*i* runs over *SC*, *SC*|*PEG*, *CC*, see Figure 7d). An important feature of activated LLPS processes in the presence of PEG or RNA, is that the backward energetic barrier toward forming metastable saturated Tau solution from the stable coacervate phase is larger than the forward barriers for forming stable coacervate droplets. Therefore, above a critical droplet size, it is unlikely that the Tau SC and Tau-RNA CC droplets can interconvert, if their formation is activated. Ostwald ripening and growth of droplets of the same type can still occur, given that the coalescence between the same droplets harboring equal viscosity does not require the dissolution of the droplet to generate free Tau in solution above a threshold concentration. Another possible scenario for droplet formation is a spinodal decomposition under conditions of high Tau concentration, in which a supersaturated Tau solution can lie in the unstable region of the phase diagram and the phase separation kinetically unlimited to create a network condensate, which can subsequently break under capillary forces and form multiple droplets. However, this scenario is not consistent with the observation of non-interconverting droplets. Taken together, the coexistence of different types of droplets in solution state suggests that both types of droplets form in the binodal phase region, and that the droplet stability and partitioning of Tau into different condensates is tuned by both thermodynamic and kinetic regulating factors.

3 | DISCUSSION

We examined the formation mechanism and properties of liquid condensates formed by Tau SC and Tau-RNA CC. Experimentally, we explored conditions under which each system forms condensates by modulating the chemical composition, salt concentration, presence of 1,6-hexanediol and temperature. We established that both SC and CC exhibit similar trends in response to these perturbations, and are driven by electrostatic interactions. The computed phase behavior of Tau SC and Tau-RNA CC by FTS shows qualitative agreement with the corresponding experimental data. We find that Tau-RNA CC has a broader two-phase region than Tau SC near physiological conditions. This result suggests that although coacervation is driven by electrostatic interactions in both cases, the presence of RNA enhances Tau

clustering and condensation. Furthermore, the fluidic properties of the liquid condensed phase starkly differ between SC and CC droplets. Specifically, the fluorescent lifetime of a covalently linked dynamics-sensitive dye found greater micro-viscosity and greater thermomechanical stability in droplets formed by Tau-RNA than by Tau SC. Also, the micro-viscosity of both SC and CC droplets substantially decreased over 24 h. A change in the fluid micro-viscosity necessarily implies a weakening of inter-molecular interactions, presumably between Tau molecules, if other solution conditions remained the same. Perhaps, depending on the type of droplet formed (SC or CC), Tau upon partitioning into the condensed phase establishes a new conformational ensemble that upon equilibration has altered long- and short-range interactions between Tau-Tau and Tau-RNA molecules. If so, why such an equilibration would take hours, and hence must be kinetically limited is unclear. Even though it is plausible that the intrinsically disordered protein Tau can establish a new conformational equilibrium in the liquid condensed phase, and the different micro-viscosity of the SC and CC droplets can be explained by Tau adopting a different conformational ensemble in the different droplets, we have no direct experimental evidence to support this idea. Notably, experimental measurement of the properties of a conformational ensemble of an IDP is exceedingly challenging. In this context, using micro-viscosity to characterize the emergent properties of different droplets over time hence could be an informative and easily accessible avenue to evaluate molecular interactions within the liquid condensed phase.

We observe that two different coacervates can coexist under a range of tuned solution conditions, but remain predominantly immiscible. This finding suggests that the droplets formed by SC versus CC of Tau must have divergent liquid properties. We rationalized the observation as a result of competition between two activated processes, each leading to a distinct LLPS state of lower free energy via an energy barrier for nucleation. Small changes in solution conditions, such as the extent of molecular crowding and RNA concentration can readily lower the energy barrier for nucleation of one of the two LLPS pathways. From this observation, we speculate that small perturbations in the cellular environment can similarly lead to large changes in the liquid condensate state that Tau exists in.

In cells, the responsive property of Tau coacervate could provide a powerful mechanism for tuning protein–protein interactions and assembly. Recent quantitative proteomics study of Tau isolated from the post-mortem human tissue identified 55 phosphorylation sites of serines, which add two negative charges per site, and

19 acetylation sites of lysines, which take away one positive charge per site. Besides charge manipulation, PTMs can vary the motif specificity for interacting partners. The combinations of these PTMs tremendously increases Tau's possible interaction modes, and also can specifically promote or inhibit the formation of one type of complex over the others. Under the condition of LLPS, abundantly present macromolecules in the cytosol such as RNA can be utilized to subtly regulate Tau condensate dynamics toward a specific state. Furthermore, the emergent fluidic properties of the condensates, and potentially the resulting shift in the conformational equilibrium of Tau, may be critical to downstream pathways including Tau aggregation, fibrillization, degradation, and sequestration. We speculate that liquid condensates that adopt properties of decreasing viscosity with time promote facile exchange of their constituents and may be more readily reversible, and hence less likely to be on pathway towards pathological and irreversible aggregation of Tau to fibrils.

ACKNOWLEDGEMENTS

AUTHOR CONTRIBUTIONS

Saeed Najafi: Conceptualization; data curation; formal analysis; methodology; validation; visualization; writing-original draft; writing-review & editing. **Yanxian Lin:** Conceptualization; data curation; formal analysis; investigation; software; validation; visualization; writing-original draft; writing-review & editing. **Andrew Longhini:** Conceptualization; data curation; formal analysis; investigation; methodology; validation; visualization; writing-original draft; writing-review & editing. **Xuemei Zhang:** Conceptualization; writing-original draft; writing-review & editing. **Kris Delaney:** Data curation; methodology. **Ken Kosik:** Conceptualization; funding acquisition; investigation; project administration; writing-review & editing. **Glenn Fredrickson:** Methodology; project administration; writing-review & editing. **Joan-Emma Shea:** Conceptualization; funding acquisition; methodology; project administration; writing-review & editing. **Songi Han:** Conceptualization; funding acquisition; investigation; methodology; writing-original draft; writing-review & editing.

ORCID

Songi Han https://orcid.org/0000-0001-6489-6246

REFERENCES

1. Eschmann NA, Georgieva ER, Ganguly P, et al. Signature of an aggregation-prone conformation of Tau. Sci Rep. 2017;7:1–10.
2. Fitzpatrick AWP, Falcon B, He S, et al. Cryo-EM structures of tau filaments from Alzheimer's disease. Nature. 2017;547:185–190.
3. Morris M, Maeda S, Vossel K, Mucke L. The many faces of tau. Neuron. 2011;70:410–426.
4. Nguyen PH, Ramamoorthy A, Sahoo BR, et al. Amyloid oligomers: A joint experimental/computational perspective on Alzheimer's disease, Parkinson's disease, type II diabetes, and amyotrophic lateral sclerosis. Chem Rev. 2021;121:2545–2647.
5. Reynolds CH, Garwood CJ, Wray S, et al. Phosphorylation regulates tau interactions with Src homology 3 domains of phosphatidylinositol 3-kinase, phospholipase Cγ1, Grb2, and Src family kinases. J Biol Chem. 2008;283:18177–18186.
6. Ittner LM, Ke YD, Delerue F, et al. Dendritic function of tau mediates amyloid-β toxicity in Alzheimer's disease mouse models. Cell. 2010;142:387–397.
7. Yamauchi PS, Purich DL. Microtubule-associated protein interactions with Actin filaments: Evidence for differential behavior of neuronal MAP-2 and tau in the presence of phosphatidylinositol. Biochem Biophys Res Commun. 1993;190:710–715.
8. He HJ, Wang XS, Pan R, Wang DL, Liu MN, He RQ. The proline-rich domain of tau plays a role in interactions with Actin. BMC Cell Biol. 2009;10:81.
9. Fulga T, Elson-Schwab I, Khurana V, et al. Abnormal bundling and accumulation of F-Actin mediates tau-induced neuronal degeneration in vivo. Nat Cell Biol. 2007;9:139–148.
10. Frandemiche ML, Seranno SD, Rush T, et al. Activity-dependent tau protein translocation to excitatory synapse is disrupted by exposure to amyloid-beta oligomers. J Neurosci. 2014;34:6084–6097.
11. Barré P, Eliezer D. Folding of the repeat domain of tau upon binding to lipid surfaces. J Mol Biol. 2006;362:312–326.
12. Zhang X, Lin Y, Eschmann NA, et al. RNA stores tau reversibly in complex coacervates. PLoS Biol. 2017;15:e2002183.
13. Ukmar-Godec T, Hutten S, Grieshop MP, et al. Lysine/RNA-interactions drive and regulate biomolecular condensation. Nat Commun. 2019;10:2909.
14. Braak H, Braak E. Neuropathological staging of Alzheimer-related changes. Acta Neuropathol. 1991;82:239–259.

15. Falcon B, Zhang W, Murzin AG, et al. Structures of filaments from Pick's disease reveal a novel tau protein fold. Nature. 2018;561:137–140.

16. Falcon B, Zivanov J, Zhang W, et al. Novel tau filament fold in chronic traumatic encephalopathy encloses hydrophobic molecules. Nature. 2019;568:420–423.

17. Zhang W, Tarutani A, Newell KL, et al. Novel tau filament fold in corticobasal degeneration. Nature. 2020;580:283–287.

18. Arakhamia T, Lee CE, Carlomagno Y, et al. Posttranslational modifications mediate the structural diversity of tauopathy strains. Cell. 2020;180:633–644.

19. Fichou Y, Lin Y, Rauch JN, et al. Cofactors are essential constituents of stable and seeding-active tau fibrils. Proc Natl Acad Sci U S A. 2018;115:13234–13239.

20. Wesseling H, Mair W, Kumar M, et al. Tau PTM profiles identify patient heterogeneity and stages of Alzheimer's disease. Cell. 2020;183:1699–1713.

21. Luo H-B, Xia Y-Y, Shu X-J, et al. SUMOylation at K340 inhibits tau degradation through deregulating its phosphorylation and ubiquitination. Proc Natl Acad Sci U S A. 2014;111:16586–16591.

22. Gamblin TC, Berry RW, Binder LI. Modeling tau polymerization in vitro: A review and synthesis. Biochemistry. 2003;42:15009–15017.

23. Reynolds MR, Berry RW, Binder LI. Site-specific nitration differentially influences τ assembly in vitro. Biochemistry. 2005;44:13997–14009.

24. Ambadipudi S, Biernat J, Riedel D, Mandelkow E, Zweckstetter M. Liquid-liquid phase separation of the microtubule-binding repeats of the Alzheimer-related protein tau. Nat Commun. 2017;8:275.

25. Hernandez-Vega A, Braun M, Scharrel L, et al. Local nucleation of microtubule bundles through tubulin concentration into a condensed tau phase. Cell Rep. 2017;20:2304–2312.

26. Wegmann S, Eftekharzadeh B, Tepper K, et al. Tau protein liquid–liquid phase separation can initiate Tau aggregation. EMBO J. 2018;37:e98049.

27. Boyko S, Qi X, Chen T-H, Surewicz K, Surewicz WK. Liquid–liquid phase separation of tau protein: The crucial role of electrostatic interactions. J Biol Chem. 2019;294:11054–11059.

28. Lin Y, McCarty J, Rauch JN, et al. Narrow equilibrium window for complex coacervation of tau and RNA under cellular conditions. Elife. 2019;8:e42571.

29. Lin Y, Fichou Y, Longhini AP, et al. Liquid-liquid phase separation of tau driven by hydrophobic interaction facilitates fibrillization of tau. J Mol Biol. 2021;433:166731.

30. Zhang X, Vigers M, McCarty J, et al. The proline-rich domain promotes Tau liquid–liquid phase separation in cells. J Cell Biol. 2020;219:e202006054.

31. Savastano A, Flores D, Kadavath H, Biernat J, Mandelkow E, Zweckstetter M. Disease-sssociated tau phosphorylation hinders tubulin assembly within tau condensates. Angew Chem Int Ed. 2021;60:726–730.

32. Burke KA, Janke AM, Rhine CL, Fawzi NL. Residue-by-residue view of in vitro FUS granules that bind the C-terminal domain of RNA polymerase II. Mol Cell. 2015;60:231–241.

33. Brady JP, Farber PJ, Sekhar A, et al. Structural and hydrodynamic properties of an intrinsically disordered region of a germ cell-specific protein on phase separation. Proc Natl Acad Sci U S A. 2017;114:E8194–E8203.

34. Lin Y, Fichou Y, Zeng Z, Hu NY, Han S. Electrostatically driven complex coacervation and amyloid aggregation of tau are independent processes with overlapping conditions. ACS Chem Nerosci. 2020;11:615–627.

35. Delaney KT, Fredrickson GH. Theory of polyelectrolyte complexation—Complex coacervates are self-coacervates. J Chem Phys. 2017;146:224902.

36. McCarty J, Delaney KT, Danielsen SPO, Fredrickson GH, Shea J-E. Complete phase diagram for liquid–liquid phase separation of intrinsically disordered proteins. J Phys Chem Lett. 2019;10:1644–1652.

37. Kroschwald S, Maharana S, Simon A. Hexanediol: A chemical probe to investigate the material properties of membrane-less compartments. Matters. 2017;3:e201702000010.

38. Molliex A, Temirov J, Lee J, et al. Phase separation by low complexity domains promotes stress granule assembly and drives pathological fibrillization. Cell. 2015;163:123–133.

39. Kroschwald S, Maharana S, Mateju D, et al. Promiscuous interactions and protein disaggregases determine the material state of stress-inducible RNP granules. Elife. 2015;4:e06807.

40. Arya S, Ganguly P, Arsiccio A, et al. Terminal capping of an amyloidogenic tau fragment modulates its fibrillation propensity. J Phys Chem B. 2020;124:8772–8783.

41. Ganguly P, Do TD, Larini L, et al. Tau assembly: The dominant role of PHF6 (VQIVYK) in microtubule binding region repeat R3. J Phys Chem B. 2015;119:4582–4593.

42. Delaney KT, Fredrickson GH. Recent developments in fully fluctuating field-theoretic simulations of polymer melts and solutions. J Phys Chem B. 2016;120:7615–7634.

43. Düchs D, Delaney KT, Fredrickson GH. A multi-species exchange model for fully fluctuating polymer field theory simulations. J Chem Phys. 2014;141:174103.

44. Fredrickson G. The equilibrium theory of inhomogeneous polymers. USA: Oxford University Press, 2006.

45. Lee J, Popov YO, Fredrickson GH. Complex coacervation: A field theoretic simulation study of polyelectrolyte complexation. J Chem Phys. 2008;128:224908.

46. Popov YO, Lee J, Fredrickson GH. Field-theoretic simulations of polyelectrolyte complexation. J Polym Sci B. 2007;45:3223–3230.

47. Villet MC, Fredrickson GH. Efficient field-theoretic simulation of polymer solutions. J Chem Phys. 2014;141:224115.

48. Doi M, Edwards SF, Edwards SF. The Theory Of Polymer Dynamics. Oxford: Oxford University Press, 1986.

49. Rubinstein M, Colby RH. Polymer Physics. Oxford, New York: Oxford University Press, 2003.

50. Mukrasch MD, Markwick P, Jacek B, et al. Highly populated turn conformations in natively unfolded tau protein identified from residual dipolar couplings and molecular simulation. J Am Chem Soc. 2007;129:5235–5243.

51. Chambers JE, Kubánková M, Huber RG, et al. An optical technique for mapping microviscosity dynamics in cellular organelles. ACS Nano. 2018;12:4398–4407.

52. Lee S-C, Heo J, Woo HC, et al. Fluorescent molecular rotors for viscosity sensors. Chem A Eur J. 2018;24:13706–13718.

53. Kuimova MK, Yahioglu G, Levitt JA, Suhling K. Molecular rotor measures viscosity of live cells via fluorescence lifetime imaging. J Am Chem Soc. 2008;130:6672–6673.

54. Panagiotou E, Millett KC, Atzberger PJ. Topological methods for polymeric materials: Characterizing the relationship between polymer entanglement and viscoelasticity. Polymers. 2019;11:437.

55. Jawerth L, Fischer-Friedrich E, Saha S, et al. Protein condensates as aging Maxwell fluids. Science. 2020;370:1317–1323.

56. Statt A, Casademunt H, Brangwynne CP, Panagiotopoulos AZ. Model for disordered proteins with strongly sequence-dependent liquid phase nehavior. J Chem Phys. 2020;152:075101.

57. Dignon GL, Zheng W, Kim YC, Best RB, Mittal J. Sequence determinants of protein phase behavior from a coarse-grained model. PLoS Comput Biol. 2018;14:e1005941.

58. Kremer K, Grest GS. Dynamics of entangled linear polymer melts: A molecular-dynamics simulation. J Chem Phys. 1990; 92:5057–5086.

59. Park S, Barnes R, Lin Y, et al. Dehydration entropy drives liquid-liquid phase separation by molecular crowding. Commun Chem. 2020;3:1–12.

SUPPORTING INFORMATION

Additional supporting information may be found online in the Supporting Information section at the end of this article.